Anisotropic Local Modification of Crystal Field Levels in Pr-Based Pyrochlores: A Muon-Induced Effect Modeled Using Density Functional Theory

F. R. Foronda,[1] F. Lang,[1] J. S. Möller,[1,*] T. Lancaster,[2] A. T. Boothroyd,[1] F. L. Pratt,[3] S. R. Giblin,[4]
D. Prabhakaran,[1] and S. J. Blundell[1,†]

[1]*Oxford University Department of Physics, Clarendon Laboratory, Parks Road, Oxford OX1 3PU, United Kingdom*
[2]*Durham University, Centre for Materials Physics, South Road, Durham DH1 3LE, United Kingdom*
[3]*ISIS Facility, Rutherford Appleton Laboratory, Chilton, Oxfordshire OX11 0QX, United Kingdom*
[4]*School of Physics and Astronomy, Cardiff University, Cardiff CF24 3AA, United Kingdom*
(Received 6 August 2014; published 6 January 2015)

Although muon spin relaxation is commonly used to probe local magnetic order, spin freezing, and spin dynamics, we identify an experimental situation in which the measured response is dominated by an effect resulting from the muon-induced local distortion rather than the intrinsic behavior of the host compound. We demonstrate this effect in some quantum spin ice candidate materials $Pr_2B_2O_7$ (B = Sn, Zr, Hf), where we detect a static distribution of magnetic moments that appears to grow on cooling. Using density functional theory we show how this effect can be explained via a hyperfine enhancement arising from a splitting of the non-Kramers doublet ground states on Pr ions close to the muon, which itself causes a highly anisotropic distortion field. We provide a quantitative relationship between this effect and the measured temperature dependence of the muon relaxation and discuss the relevance of these observations to muon experiments in other magnetic materials.

The muon-spin relaxation (μSR) technique has been widely used as a probe of exotic magnetic behavior in frustrated systems [1]. A crucial question for these experiments is to what extent the presence of an implanted muon perturbs its local environment to such a degree that the measured response no longer reflects the physical behavior of the system under study. To answer this question we have identified a worst-case scenario, where the intrinsic magnetic behavior is that of a quantum spin ice originating from the magnetic moments of Pr^{3+} ($4f^2$) ions but the effect of the muon on the local environment dramatically alters the observed behavior. The ground state doublet of this non-Kramers ion due to the high symmetry of the Pr^{3+} site is particularly susceptible to modification by the implanted muon (in contrast, a Kramers ion must have a doublet ground state, whatever the site, and this doublet cannot be split by any perturbation that does not break time-reversal symmetry). By using density-functional-theory (DFT) and crystal-field (CF) calculations, we show in this Letter how the observed behavior results from a highly anisotropic distortion field induced by the implanted muon.

In pyrochlore oxides $A_2B_2O_7$, in which the magnetic A ions occupy a lattice of corner-sharing tetrahedra, a variety of ground states can be realized, including spin glasses and spin ices [2]. Spin-ice behavior has been widely studied in $Dy_2Ti_2O_7$ and $Ho_2Ti_2O_7$ (i.e., with A = Dy or Ho and B = Ti) and arises because the Ising spins are constrained by the CF to point in or out of each tetrahedron and along the local $\langle 111 \rangle$ axes [3,4]. It has been suggested that a new type of quantum spin ice [5] may be realized in which A is a

lanthanide with fewer f electrons and a smaller magnetic moment, such as Pr^{3+} [6,7]. This leads to a spatially extended $4f$ wave function with a greater overlap with the oxygen $2p$ orbitals, as well as a weaker magnetic dipolar interaction (proportional to the square of the moment size) between nearest-neighbor sites. This can allow quantum tunneling between different ice configurations, thereby converting the material from a spin ice to a quantum spin liquid. Like its classical counterpart, the most notable feature of this new state is that it is predicted to host unconventional excitations. These are linearly dispersive magnetic excitations (magnetic photons), which offer the possibility of constructing a real lattice analogue of quantum electromagnetism [8,9]. The compound $Pr_2Ir_2O_7$ has been identified as a highly correlated metallic spin liquid [10,11] and a previous μSR investigation found behavior that was interpreted as being induced by the muon [12,13], although the extent of the role of screening by the conduction electrons was not clear. We now demonstrate that this effect can be also found in the insulating compounds $Pr_2B_2O_7$ (B = Sn, Zr, and Hf), which are also candidate quantum spin ice systems, and we propose a theoretical description for the observed effect.

Zero-field μSR measurements were carried out on polycrystalline samples mainly using the EMU spectrometer at the ISIS muon facility, Rutherford Appleton Laboratory (RAL), but also the GPS spectrometer at the Swiss Muon Source (PSI). Data were taken in the temperature range 0.05–280 K using a ^{3}He cryostat and ^{3}He-^{4}He dilution refrigerator. The samples were synthesized by

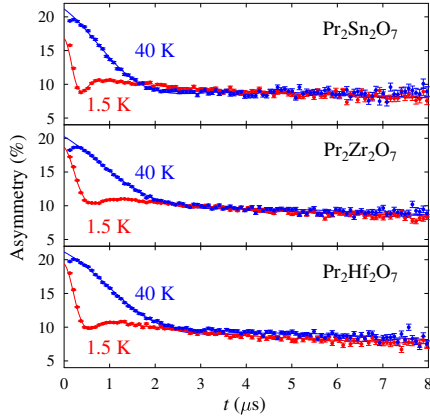FIG. 1 (color online). Zero-field μSR spectra at 1.5 and 40 K. Fits are to a Kubo-Toyabe relaxation function.
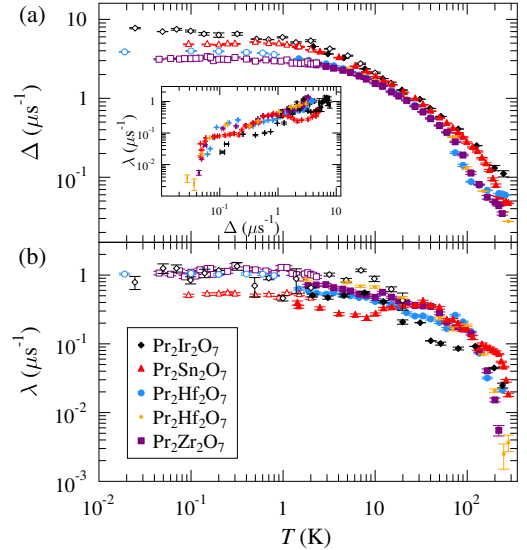

FIG. 2 (color online). Temperature dependences of (a) Δ and (b) λ in Pr-based pyrochlores (helium cryostat, filled symbols; dilution fridge, open symbols). The two data sets for $Pr_2Hf_2O_7$ were taken with the same sample but in separate experiments to check reproducibility. The $Pr_2Ir_2O_7$ data are taken from Ref. [12].

standard solid-state reactions and confirmed by x-ray diffraction to be single phase. Representative raw spectra from μSR measurements taken in zero applied field at 1.5 and 40 K are shown in Fig. 1. At 1.5 K all compounds show a Kubo-Toyabe relaxation function (an initially Gaussian depolarization, which recovers to a $\frac{1}{3}$ constant long-time tail), which can be understood as resulting from a distribution of randomly oriented, static magnetic moments [14]. The static moments lead to a Gaussian distribution of magnetic fields at the muon site of rms width $B_{rms} = \Delta/\gamma_\mu$, where $\gamma_\mu = 2\pi \times 135.5$ MHz T^{-1} is the muon gyromagnetic ratio. However, the value of Δ extracted at low temperature appears to be too large to originate simply from nuclear spins. We fit our data to a product of a Gaussian Kubo-Toyabe function $G_{KT}(\Delta, t)$ [14] and a weakly relaxing exponential $e^{-\lambda t}$, the latter component to take into account some slow dynamics of the magnetic moments, and this fit function can be used across the entire temperature range studied. All samples show a small, rapidly relaxing fraction, which we interpret as a muonium state (and which is responsible for the negative curvature in the asymmetry data at very short times), but we focus on the majority fraction in the subsequent discussion.

The temperature dependences of the static width Δ and dynamic relaxation rate λ are shown in Fig. 2. No magnetic transition can be seen throughout the measured temperature range; both parameters evolve smoothly, increasing steadily as the samples are cooled, and the increase in Δ can be interpreted as magnetic moments, which grow with decreasing temperature. The two parameters λ and Δ roughly track each other (see inset to Fig. 2), suggesting that the dynamics are related to these growing moments. The values of B_{rms} extrapolated to zero temperature (see Table I) are found to be an order of magnitude larger than expected from ^{141}Pr nuclear moments [12,13] and are larger for smaller lattice constants a.

In these quantum spin ice systems we do not expect any static electronic moments at any temperature.

Nuclear moments would be expected to give a small temperature-independent Δ, but the observed behavior in Fig. 2(a) is both strongly temperature dependent and at low temperatures very large. A likely explanation comes via a hyperfine enhancement of the Pr nuclear moments (as proposed for $Pr_2Ir_2O_7$ [12,13] and discussed in more detail below), but this mechanism requires a nonmagnetic (singlet) ground state. In the pyrochlore structure the Pr^{3+} ($4f^2$) ground state is a well isolated non-Kramers doublet (confirmed in $Pr_2Sn_2O_7$ and $Pr_2Zr_2O_7$ by neutron spectroscopy [15,16]) but this could be split by the distortion introduced by the muon. A muon-induced perturbation of the CF has been suggested previously in Pr-based intermetallics [17,18], although in those cases the ground state is already a singlet due to lower symmetry and the effect is only on the excited CF levels. Since our data in insulating pyrochlores look very similar to those in metallic $Pr_2Ir_2O_7$ we conclude that this mechanism is not very sensitive to conduction-electron screening effects. In fact, the carrier density in $Pr_2Ir_2O_7$ is found to be rather low

TABLE I. Lattice constants a (at 300 K), rms field width B_{rms}, and fitted energy gaps ϵ_i (see later) for $Pr_2B_2O_7$ (B = Zr, Hf, Sn, and Ir). $Pr_2Ir_2O_7$ data are taken from Refs. [10,12].

Compound	Zr	Hf	Sn	Ir
a (Å)	10.7386(2)	10.7177(2)	10.6055(2)	10.3940(4)
B_{rms} (mT)	3.76(6)	4.4(1)	5.65(5)	8.9(4)
ϵ_1 (meV)	3.1(5)	2.1(7)	6(1)	0.5(1)
ϵ_2 (meV)	0.6(1)	0.3(2)	0.6(1)	0.1(1)

(estimated to be 2.6×10^{20} cm^{-3}, i.e., ≈ 0.02 conduction electrons per Pr, from Hall effect measurements [10]). Moreover, $Pr_2Ir_2O_7$ is believed to have a Fermi node at the Γ point [19], so that conduction electrons can only screen effectively at very long wavelengths. However, $Pr_2Ir_2O_7$ has the largest B_{rms} in Table I, which we show below is related to the smallest doublet splitting and distortion, so screening effects may play some small role.

Although there has been previous evidence for a muon-induced effect in Pr-containing systems with a non-Kramers doublet [12,17,18], the nature of the effect has not been explored in detail. To address this issue we have used DFT calculations to determine the muon location and assess the effect of the muon on the local crystal structure and the CF of nearby Pr ions. DFT calculations were conducted with the plane-wave QUANTUM ESPRESSO[20] program utilizing the generalized gradient approximation exchange-correlation functional [21]. Ions were modeled using ultrasoft pseudopotentials and the muon was modeled by a norm-conserving hydrogen pseudopotential. This technique is known to give reliable results for muon sites in condensed matter systems [22–24]. Two different Pr pseudopotentials were used, with the $4f$ electrons either in valence or in the core. The resulting muon stopping sites and bulk lattice parameters were found to agree in both cases, probably due to the muon forming an O–H type bond (see below) making it insensitive to the modeling of the Pr $4f$ electronic configuration. Hence, a Pr pseudopotential with the $4f$ electrons in the core, which is less computationally demanding, was employed for the calculations described below. The calculations were performed for $Pr_2Sn_2O_7$ in a supercell consisting of a single conventional unit cell containing 88 atoms, and with the total energy converged to at least 1×10^{-6} Ry/atom (where Ry is the Rydberg constant). A convergence test yielded the suitable wave function and charge density cutoffs of 50 and 300 Ry, respectively, on a $2 \times 2 \times 2$ Monkhorst-Pack k-space grid, which were then used in all subsequent calculations. The calculated atomic positions and lattice parameter of the unperturbed bulk were within 2% of the experimental values reported in Ref. [25]. A muon was introduced on a grid of low-symmetry positions and the system was allowed to relax until all forces were below 10^{-3} Ry/a.u. and the change in energy between iterations was less than 10^{-4} Ry. The calculations presented here focus solely on the diamagnetic muon state, for which the unit cell has a total charge of $+1$. The final relaxed positions were found to be the same in spin-polarized and nonpolarized calculations.

Three potential stopping sites were identified. However, as two of these required configurations that were ~0.45 and 0.9 eV higher in energy than that of the lowest state we conclude that the latter is the most plausible stopping site in our real system. In this scenario the muon forms a O–H type bond of length ≈ 1 Å. It is bonded to an O^{2-} ion, which
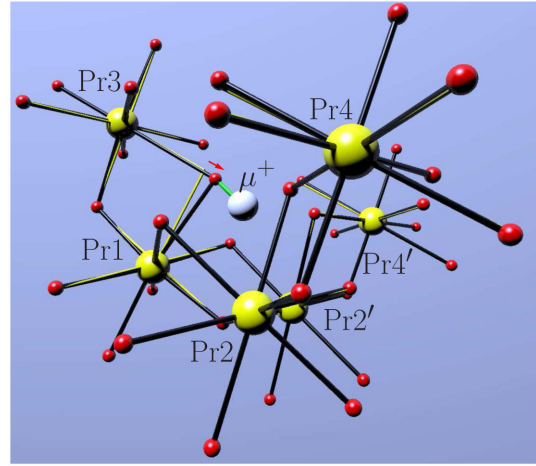

FIG. 3 (color online). Muon stopping site (white sphere) and atomic positions in $Pr_2Sn_2O_7$ as calculated by DFT. Oxygen sites are shown in red, Pr ions are shown in yellow, and bonds are shown as solid black lines. Bonds of the unperturbed lattice (yellow lines) are included for comparison. Pr ions are numbered in order of separation from μ with Pr1 being the closest. The pair Pr2 and Pr 2′ is equidistant from the muon, as are Pr4 and Pr 4′.

also bonds to two Pr ions, labeled Pr1 and Pr3 in Fig. 3 (the Pr ions in Fig. 3 are numbered in order of separation from the muon, with Pr1 being the closest). The implanted muon results in an anisotropic distortion of the crystal lattice. The muon pulls an O^{2-} away from the ion Pr3, resulting in a greatly extended Pr3–O bond. The Pr1–O bond is only slightly changed in length, but is bent round, resulting in an anisotropic distribution of O^{2-} ions around Pr1. As shown below, the largest change in the CF ground state is found for Pr3, but we note that the environment around the ions labeled Pr2, Pr 2′, Pr4, and Pr 4′ is more gently modified.

We quantify the relative distortion of a PrO_8 unit as the rms of the differences in Pr–O bond lengths between the perturbed and unperturbed lattice and these are listed in Table II for each of the nearest sites. We have calculated the CF levels for all nearby PrO_8 environments, taking into account the spatial arrangement of the eight nearest-neighbor oxygen anions around each Pr (the electrostatic field due to the muon itself was also included initially, but it was found to make little difference, and so was neglected for the calculations described here). We used a point-charge

TABLE II. Parameters derived from DFT calculations of muon-induced lattice perturbations in $Pr_2Sn_2O_7$. Values are shown for the four nearest-neighbor Pr ions.

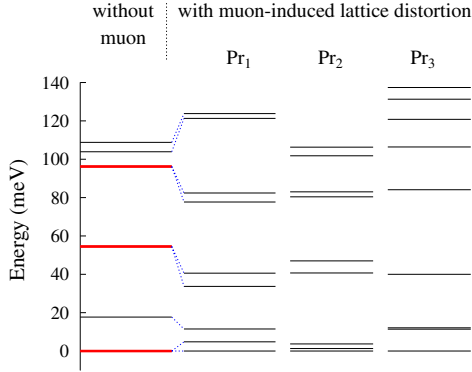| Pr atom	1	2, 2′	3	4, 4′
Pr–μ separation (Å)	2.7	3.2	4.1	4.7
Relative contribution	0.45	1.0	0.05	0.10
Distortion of PrO_8 unit (Å)	0.23	0.07	0.56	0.09
ϵ (meV)	4.8	1.3	11.4	4.0

FIG. 4 (color online). Calculated CF levels of Pr^{3+} with and without muon-induced lattice distortion in $Pr_2Sn_2O_7$. Energies are calculated for three Pr^{3+} sites with varying degrees of distortion (see Table II) as determined by DFT calculations. Bold red lines indicate doublets; plain black lines are singlets.

FIG. 5 (color online). Static relaxation rate Δ fitted with the model described in the text. The symbols are the same as in Fig. 2.

model, with effective charges on the O1 and O2 sites chosen to reproduce the measured CF spectrum [15]. For each Pr site, the muon-induced distortion splits the non-Kramers ground state doublet into two singlets (Fig. 4). These calculations show that the most perturbed Pr ion is not that nearest to the muon (there are three closer Pr ions that are significantly less perturbed), reflecting the highly anisotropic nature of the induced distortion field. Thus, we conclude that the muon is surrounded by a number of close Pr ions in which the CF splitting varies considerably.

We now turn to the hyperfine enhancement of the Pr nuclear spins caused by these CFs. One can consider a two-state model due to Bleaney [26] in which the non-Kramers doublet is split into two singlets $|G\rangle$ and $|E\rangle$ by a small energy ϵ. For a nucleus with spin $\boldsymbol{I}$ the Hamiltonian takes the form

$$\mathcal{H} = \mathcal{H}_X + g_J\mu_B\boldsymbol{B}\cdot\boldsymbol{J} + A_J\boldsymbol{J}\cdot\boldsymbol{I} - g_I\mu_B\boldsymbol{B}\cdot\boldsymbol{I}. \quad (1)$$

Here, the field $\boldsymbol{B}$ is applied along the z direction and $\mathcal{H}_X$ accounts for the CF and the splitting ϵ. There is an electronic matrix element $\alpha = \langle E|\hat{J}_z|G\rangle$, where $\hat{J}_z$ is the electronic angular momentum. This model allows an estimate of the magnetic moment $m = k_B T(\partial\ln Z/\partial B)_T$ where Z is the partition function, and yields $m = g_I\mu_B I_z + g_J\mu_B\alpha\sin\theta\tanh(\epsilon/2\cos\theta k_B T)$, where $\tan\theta = 2\alpha(g_I\mu_B B_z + A_J I_z)/\epsilon$. In zero-field μSR we take $B_z = 0$ and hence

$$m = m_0 + \frac{\eta}{\tilde{\epsilon}}\tanh\left(\frac{\tilde{\epsilon}}{k_B T}\right), \quad (2)$$

where $m_0 = g_I\mu_B I_z$, $\eta = g_J\mu_B\alpha^2 A_J I_z$, and $\tilde{\epsilon} = \sqrt{(\epsilon/2)^2 + (\alpha A_J I_z)^2}$ (where $\alpha^2 \leq J^2$). Taking $\Delta \propto m$ with $A_J/h = 1.093$ GHz [26] and $I_z = \frac{5}{2}$ allows an estimate of the upper bound of ϵ. The muon is coupled to many neighboring moments by the dipole-dipole interaction,
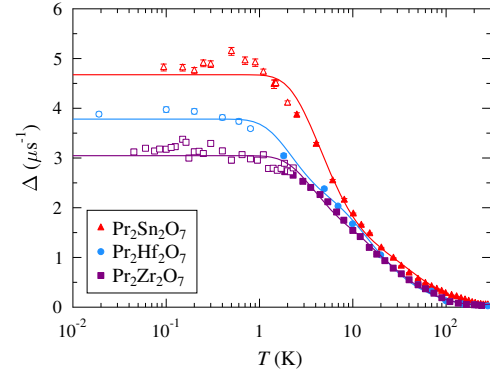
which is proportional to r^{-3} (the relative contribution of this coupling for each site is listed in Table I, assuming a r^{-3} dependence and the induced moment $\propto \epsilon^{-1}$). For simplicity, we choose a model in which there are dominant contributions to Δ from two nearby moments, which act in quadrature. We note that Eq. (2) implies that (neglecting the m_0 component and for $\epsilon \gg \alpha^2 A_J I_z$) the enhanced moment is approximately inversely proportional to ϵ at low temperature, and therefore we expect the response to be dominated by nearby sites with small splittings. The zero-field data sets for all compounds are found to fit well to this two-component model, see Fig. 5. The fitted values for all compounds are listed in Table II. We note that these values are within the same order of magnitude as our estimated splittings for the nearest neighbor sites Pr1, and Pr2 or Pr 2′ for $Pr_2Sn_2O_7$. Given the sensitivity of the calculations to the precise distortion field, the restriction to two components, together with the limitations of the point-charge model of the CF, we believe this agreement is well within the inherent uncertainties.

In conclusion, our observations show that, in certain circumstances, μSR experiments can measure a response that is dominated by the local distortion resulting from the implanted probe rather than the intrinsic behavior of the sample. The particular case of $Pr_2B_2O_7$ is unusual since the effect relies on a splitting of a non-Kramers doublet in high symmetry Pr^{3+}. This mechanism would be inoperable in systems in which the ground state degeneracy was protected from such perturbations, such as in $Dy_2Ti_2O_7$, where a similar anisotropic distortion field will nevertheless be induced but will only serve to modify the excited CF levels and will not split the Kramers doublet ground state. Our work implies that in any oxide there will always be an anisotropic distortion field around the implanted muon (which we have shown can be modeled using DFT) and its effect should always be considered. In magnetically ordered materials these distortions will have minimal effect because the coupling of the muon to the local magnetic field dominates. If frustration or low dimensionality leads

to a less robust ground state then particular care is needed, and especially in the case of high-symmetry non-Kramers doublet ground states, which are most susceptible to these muon-induced effects.

[*]Laboratory for Solid State Physics, ETH Zürich, Zürich, Switzerland.

[†]s.blundell@physics.ox.ac.uk

[1] P. Carretta and A. Keren, in *Highly Frustrated Magnetism*, edited by C. Lacroix, P. Mendels, and F. Mila (Springer, New York, 2011), pp. 79–106.

[2] J. S. Gardner, M. J. P. Gingras, and J. E. Greedan, Rev. Mod. Phys. **82**, 53 (2010).

[3] S. T. Bramwell and M. J. P. Gingras, Science **294**, 1495 (2001).

[4] C. Castelnovo, R. Moessner, and S. L. Sondhi, Nature (London) **451**, 42 (2008).

[5] M. J. P. Gingras and P. A. McClarty, Rep. Prog. Phys. **77**, 056501 (2014).

[6] S. Onoda and Y. Tanaka, Phys. Rev. Lett. **105**, 047201 (2010).

[7] H. D. Zhou, C. R. Wiebe, J. A. Janik, L. Balicas, Y. J. Yo, Y. Qiu, J. R. D. Copley, and J. S. Gardner, Phys. Rev. Lett. **101**, 227204 (2008).

[8] O. Benton, O. Sikora, and N. Shannon, Phys. Rev. B **86**, 075154 (2012).

[9] S. B. Lee, S. Onoda, and L. Balents, Phys. Rev. B **86**, 104412 (2012).

[10] S. Nakatsuji, Y. Machida, Y. Maeno, T. Tayama, T. Sakakibara, J. vanDuijn, L. Balicas, J. N. Millican, R. T. Macaluso, and J. Y. Chan, Phys. Rev. Lett. **96**, 087204 (2006).

[11] Y. Tokiwa, J. Ishikawa, S. Nakatsuji, and P. Gegenwart, Nat. Mater. **13**, 356 (2014).

[12] D. E. MacLaughlin, Y. Ohta, Y. Machida, S. Nakatsuji, G. Luke, K. Ishida, R. Heffner, L. Shu, and O. Bernal, Physica (Amsterdam) **404B**, 667 (2009).

[13] D. E. MacLaughlin, Y. Nambu, Y. Ohta, Y. Machida, S. Nakatsuji, and O. O. Bernal, J. Phys. Conf. Ser. **225**, 012031 (2010).

[14] R. S. Hayano, Y. J. Uemura, J. Imazato, N. Nishida, T. Yamazaki, and R. Kubo, Phys. Rev. B **20**, 850 (1979).

[15] A. J. Princep, D. Prabhakaran, A. T. Boothroyd, and D. T. Adroja, Phys. Rev. B **88**, 104421 (2013).

[16] K. Kimura, S. Nakatsuji, J.-J. Wen, C. Broholm, M. B. Stone, E. Nishibori, and H. Sawa, Nat. Commun. **4**, 1934 (2013).

[17] R. Feyerherm, A. Amato, A. Grayevsky, F. Gygax, N. Kaplan, and A. Schenck, Z. Phys. B **99**, 3 (1995).

[18] T. Tashma, A. Amato, A. Grayevsky, F. N. Gygax, M. Pinkpank, A. Schenck, and N. Kaplan, Phys. Rev. B **56**, 9397 (1997).

[19] L. Savary, E.-G. Moon, and L. Balents, Phys. Rev. X **4**, 041027 (2014).

[20] P. Giannozzi *et al.*, J. Phys. Condens. Matter **21**, 395502 (2009).

[21] J. P. Perdew, K. Burke, and M. Ernzerhof, Phys. Rev. Lett. **77**, 3865 (1996).

[22] J. S. Möller, D. Ceresoli, T. Lancaster, N. Marzari, and S. J. Blundell, Phys. Rev. B **87**, 121108 (2013).

[23] F. Bernardini, P. Bonfà, S. Massidda, and R. De Renzi, Phys. Rev. B **87**, 115148 (2013).

[24] S. J. Blundell, J. S. Möller, T. Lancaster, P. J. Baker, F. L. Pratt, G. Seber, and P. M. Lahti, Phys. Rev. B **88**, 064423 (2013).

[25] B. J. Kennedy, B. A. Hunter, and C. J. Howard, J. Solid State Chem. **130**, 58 (1997).

[26] B. Bleaney, Physica (Amsterdam) **69**, 317 (1973).